Proceedings of IMECE2005
2005 ASME International Mechanical Engineering Congress and Exposition
November 5-11, 2005, Orlando, Florida USA

IMECE2005-80511

NEW APPROACHES FOR SAMPLE-PROFILE ESTIMATION FOR FAST ATOMIC FORCE MICROSCOPY

Srinivasa M Salapaka *
Mechanical and Industrial Engineering
University of Illinois
Urbana, IL 61801
Email: salapaka@uiuc.edu

Tathagata De
Electrical and Computer Engineering
Iowa State University
Ames, IA 50011
tatha@iastate.edu

Abu Sebastian
IBM Zurich Research Laboratory
CH-8803 Rüschlikon
Switzerland
ase@zurich.ibm.com

ABSTRACT

The Atomic Force Microscope (AFM) is a powerful tool for imaging and manipulating matter at the nanoscale. The sample-profile estimation problem in Atomic Force Microscopy is addressed using $\mathcal{H}_\infty$ control. A new estimate signal for the sample profile is proposed and it is proved that this signal tracks perfectly the profile signal. i.e., the transfer function between the profile signal and the estimate signal is one. Experimental results are presented to corroborate these results.

Introduction

Recently there has been moderate effort to improve the Atomic Force Microscopes (AFMs) in terms of their scanning speeds. This effort forms a main component of research striving to achieve robust broadband nanopositioning and imaging in order to realize the goal of interrogating and manipulating matter at the nanoscale at reasonable time scales. Most of the commercial devices at present predominantly employ ad-hoc methods that result in large deficits in achievable bandwidth as they fail to address the multi-objective concerns of nonlinear behavior of piezoelectric actuators, coupling effects, the effects of positioner dynamics on imaging and the uncertain and diverse environments. Recent research in systems community has developed design which have improved significantly the bandwidths for lateral positioning in these devices. This has necessitated the search for obtaining signals that give faithful images of the samples when scanned at fast speeds.

There has been a growing interest in Atomic Force Microscopy in the Systems community. Their contribution has been in analysis, modelling, and improving device performance. System and dynamic systems concepts have also been used in studying microcantilevers and analyzing their interactions with sample surfaces. System tools have been used to study steady state behaviors of cantilevers [1,2], explain rich complex behavior observed in experiments [3,4], and derive fundamental limitations on this technology [5]. The system identification techniques have been used to provide mathematical models of the system without having the need to deal with the complex geometry or material composition of the device [6–10]. The fine resolution and large range of motion for these devices are typically provided by piezo-actuators. However, piezo-actuation introduces effects such as hysteresis, drift and creep which adversely affect the performance of the device. System tools have been applied to study these effects and compensate for them [10]. The (PID)-design, which is typically employed for control in these devices is inadequate, in many cases, to realize their full potential. Consequently, Robust control tools have been proposed and implemented which have shown substantial improvement in *simultaneously* achieving fine resolution, high bandwidth and robustness of these devices [7,8]. The need for high throughputs in many applications has imposed severe demands on these devices. Several system theoretic methods are being applied to address this need, for e.g., increasing the detection bandwidth using observer based control scheme in [11]; and increasing the throughput by implementing an array of cantilevers by using analysis and control tools from the area of distributed control theory [12,13].

*Address all correspondence to this author.

In this paper, we address the problem of obtaining accurate estimates of the sample-surface profiles, especially for fast imaging applications. It forms an important step towards building a robust high precision microscope with ultrafast imaging capability. Typically, the control signal u which is the input to the vertical positioner is used as an estimate for the profile, which provides good images for slow scans but proves to be unsatisfactory for fast scans of rough surfaces (since vertical piezo dynamics get excited at fast scanning speeds). The main contribution of this paper is that we propose a new estimate signal (in place of the control signal) and prove that it asymptotically tracks the profile perfectly for *all* frequencies - i.e., the transfer function between the estimate signal and the sample profile signal is equal to one! The proposed signal is obtained by exploiting the 'quasi-observer' form of the central $\mathcal{H}_\infty$-controller and the structure of the model for the device. It comes at no extra computational cost over the control design - The $\mathcal{H}_\infty$ controller is designed to obtain set point regulation and high resolution and the proposed profile estimate signal is derived in terms of this controller. This scheme is demonstrated by simulation and experimental results.

An optimal control problem is proposed which includes the objectives of high resolution, set point regulation and low profile estimation error. We show that the proposed signal is a solution to this problem and study its robustness to modeling uncertainties. In context of using a model for vertical positioners to obtain profile estimates this paper presents an analysis of profile estimate signals based on observer control designs and studies their robustness to modeling uncertainties and contrasts them with the proposed signal.

1 Motivation and Optimal Control Problem Formulation

A schematic of an AFM and its working principle is illustrated in Figure 1. In a typical contact mode operation, the cantilever deflection is regulated at a set-point (i.e. the tip-sample force is kept constant) while scanning the sample. This is achieved by moving the vertical positioner (Z-piezo) to which the cantilever is attached up or down to compensate for the undulations in the sample surface by using a feedback controller. The input to the vertical positioner, i.e. the compensating control signal, is traditionally used as a measure of the sample profile.

However, this method of imaging is valid only for low bandwidth imaging applications. Figure 2 shows a system theoretic model of an AFM. Here G_z represents the vertical positioner, G_c represents the microcantilever, S_D represents the deflection transducer and K is the control transfer function. The cantilever tip encounters the surface topography as a time signal $d(t) = h(x(t), y(t))$ where $h(\cdot,\cdot)$ represents the sample profile and $(x(t), y(t))$ denotes the lateral coordinates of the tip sample contact point set by the X-Y scanner. This sample profile signal d is viewed as a "disturbance" signal which tries to deviate

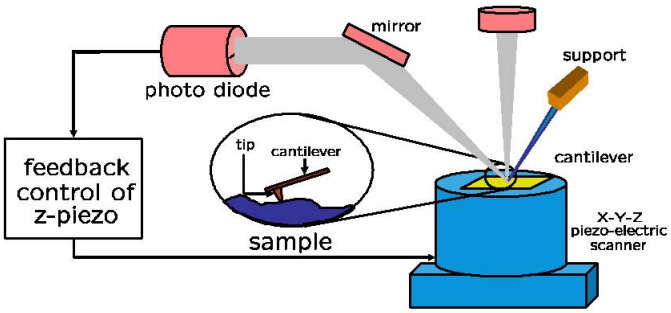

Figure 1. A SCHEMATIC OF AN AFM.

the cantilever deflection signal from its set point deflection (see Figure 2-(A)). The signals r, y, e and n are the setpoint, the cantilever deflection, the deflection error and the transducer noise respectively. We simplify this diagram by combining the transfer functions G_z, G_c and S_D^{-1} as in Figure 2(B). If we assume that G_c is equal to a constant S_C (which is a good approximation since micro-cantilevers have much larger bandwidths than the vertical scanners), then $\tilde{d}$ represents a scaled sample profile.

The inadequacy of the control signal as an imaging signal at high frequencies is explained by looking at the requirements on control design. It is required that there is good set point regulation to avoid tip-sample damage and to retain the validity of the model. A good set point regulation over a pre-specified bandwidth is achieved by designing K to have high gain over the bandwidth. This is easily seen from the transfer function from set point r to the regulation error e given by the sensitivity function $S = \frac{1}{1+G(j\omega)K(j\omega)}$ which is small when $|K(j\omega)|$ is large. Moreover the transfer function from the sample profile $\tilde{d}$ to the control signal u is $\frac{K(j\omega)}{1+K(j\omega)G(j\omega)}$ which is $\approx \frac{1}{G(j\omega)}$ for large K. Typically the positioner transfer function $G(j\omega)$ is approximately a constant at low frequencies and thus the control signal u is a good estimate of the sample profile. However at high frequencies $G(j\omega)$ is not constant and the dynamics of the positioner has to be dealt with. The control signal is clearly an inaccurate estimate of the sample profile at these frequencies. Also note that the temporal frequency content of the $\tilde{d}$ depends on the spatial frequency content of the sample, i.e. how *rough* the sample is, and the scanning rate of the lateral positioners, i.e how *fast* the sample is scanned. In the view of new control designs [8, 9, 14, 15] for faster lateral positioning it is imperative to obtain better estimates of $\tilde{d}$ especially with high frequency content.

It needs to be emphasized that the ultimate goal of microscopy is imaging; the resolution and regulation objectives are futile if the imaging objective is not achieved. In this context, we lay down an optimal control problem which captures all the objectives (See Figure 3) - (a) set-point regulation to avoid image

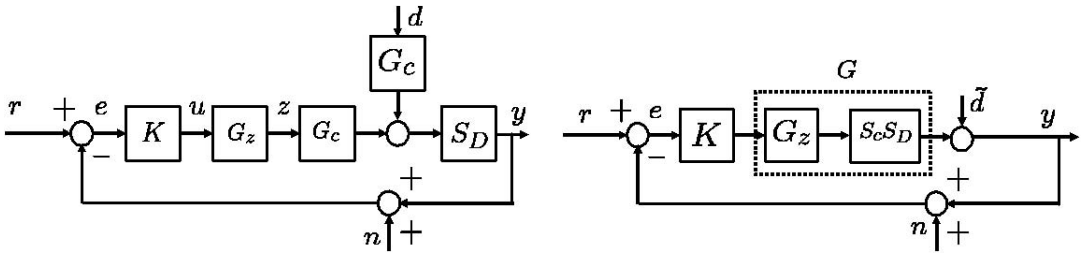

Figure 2. (A) THE BLOCK DIAGRAM MODELING OF THE AFM. (B) G REPRESENTS A COMBINATION OF THE SCANNER, LEVER AND THE TRANSDUCER DYNAMICS. $\tilde{d}$ IS A SCALED VERSION OF THE SAMPLE TOPOGRAPHY

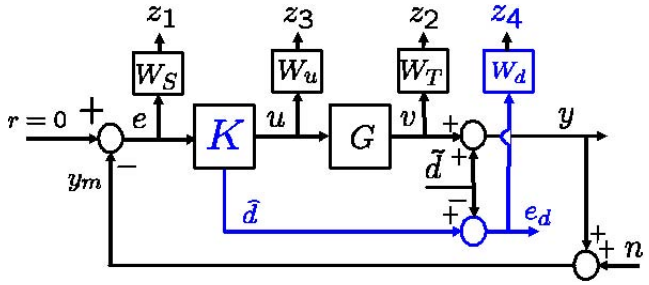

Figure 3. FRAMEWORK FOR THE OPTIMAL CONTROL PROBLEM.

distortions, (b) high frequency noise rejection for high resolution, (c) low control effort to avoid piezo saturation and (d) minimizing sample profile estimation error. In this formulation, the set point regulation, the high resolution and bounded control objectives are captured by the regulated outputs $z_1 = W_S e$, $z_2 = W_T v$ $z_3 = W_u u$ and $z_4 = W_d e_d$ where W_S, W_T and W_u are appropriately chosen weighting functions [16]. The main contribution of this paper is addressing the objective of finding a sample profile estimate. This is captured by requiring the estimate error $W_d(\hat{d} - \tilde{d})$ to be small. Thus the transfer function P from $[r-n\ \tilde{d}]^T$ to z is described by

$$\begin{bmatrix} z_1 \\ z_2 \\ z_3 \\ z_4 \end{bmatrix} = \begin{bmatrix} W_S S & -W_S S \\ W_T T & -W_T T \\ W_u K_1 S & -W_u K_1 S \\ W_d K_2 S & -W_d(1+K_2 S) \end{bmatrix} \begin{bmatrix} r-n \\ \tilde{d} \end{bmatrix} \tag{1}$$

where $S = \frac{1}{1+GK_1}$ is the sensitivity and $T = 1-S$ is the complementary sensitivity function. These multiple objectives on control design are met by solving the following $\mathcal{H}_\infty$ problem:

$$arg \min_{K=[K_1\ K_2]^T} \|P\|_\infty. \tag{2}$$

In practice, for the sake of computational simplicity, we relax this problem in which we seek a sub optimal controller that satisfies $\|P\|_\infty < \gamma$ for some $\gamma > \min_K \|P\|_\infty$. Note that the optimal control problem seeks a *two by one* transfer function $K = [K_1\ K_2]^T$ where K_1 decides set point regulation, resolution and control within saturation objectives while K_2 decides the extent of sample estimation error.

1.1 Proposed Sample-Profile Signal

In this section we prescribe a profile estimate signal $\hat{d}$. The main features of this signal is that it gives a perfect tracking of the sample profile in the sense that the transfer function from profile $\tilde{d}$ to $\hat{d}$ is equal to one!

The signal $\hat{d}$ is obtained by analyzing the $\mathcal{H}_\infty$ feedback law designed only for the first three objectives, i.e. $\left\| \begin{matrix} W_S S \\ W_T T \\ W_u K_1 S \end{matrix} \right\|$ and exploiting its quasi-observer structure. It also exploits that the disturbance signal enters the plant G dynamics only in its output and not in its state evolution equation. If the state-space representations of G and the weighting functions are given by

$$G = \left[\begin{array}{c|c} A_g & B_g \\ \hline C_g & D_g \end{array}\right],\ W_S = \left[\begin{array}{c|c} A_s & B_s \\ \hline C_s & D_s \end{array}\right],\ W_T = \left[\begin{array}{c|c} A_t & B_t \\ \hline C_t & D_t \end{array}\right] \text{ and } W_u = \left[\begin{array}{c|c} A_u & B_u \\ \hline C_u & D_u \end{array}\right] \tag{3}$$

then the corresponding generalized plant P is described by:

$$\begin{bmatrix} \dot{x_g} \\ \dot{x_s} \\ \dot{x_t} \\ \dot{x_u} \end{bmatrix} = \underbrace{\begin{bmatrix} A_g & & & \\ -B_s C_g & A_s & & \\ B_t C_g & 0 & A_t & \\ & & & A_u \end{bmatrix}}_{\triangleq A} \underbrace{\begin{bmatrix} x_g \\ x_s \\ x_t \\ x_u \end{bmatrix}}_{\triangleq x} + \underbrace{\begin{bmatrix} 0 \\ B_s \\ 0 \\ 0 \end{bmatrix}}_{\triangleq B_1} w + \underbrace{\begin{bmatrix} B_g \\ -B_s D_g \\ B_t D_g \\ B_u \end{bmatrix}}_{\triangleq B_2} u \tag{4}$$

$$\begin{bmatrix} z_1 \\ z_2 \\ z_3 \end{bmatrix} = \underbrace{\begin{bmatrix} -D_s C_g & C_s & & \\ D_T C_g & 0 & C_t & \\ & & & C_u \end{bmatrix}}_{\triangleq C_1} \begin{bmatrix} x_g \\ x_s \\ x_t \\ x_u \end{bmatrix} + \underbrace{\begin{bmatrix} D_s \\ 0 \\ 0 \end{bmatrix}}_{\triangleq D_{11}} w + \underbrace{\begin{bmatrix} -D_s D_g \\ D_t D_g \\ D_u \end{bmatrix}}_{\triangleq D_{12}} u$$

$$e = \underbrace{\begin{bmatrix} -C_g & 0 & 0 & 0 \end{bmatrix}}_{\triangleq C_2} \begin{bmatrix} x_g \\ x_s \\ x_t \\ x_u \end{bmatrix} + \underbrace{[I]}_{\triangleq D_{21}} w - \underbrace{D_g}_{\triangleq D_{22}} u,$$

where $w = r - n - \tilde{d}$ (Here we consider set point r to be 0 without any loss of generality and do not consider the effect of noise n. Its effect is considered in the next section). The $\mathcal{H}_\infty$ synthesis procedure ([16], [17], [18]) yields a controller K_1 which can be written as an observer-based state feedback

$$\dot{\hat{x}} = (A + B_1 F_{12\infty} + Z_\infty L_{2\infty} F_{12\infty})\hat{x} + B_2 u + Z_\infty L_{2\infty}(\underbrace{C_2\hat{x} + D_{22}u}_{\triangleq \hat{e}} - e) \quad (5)$$

$$u = F_{2\infty}\hat{x}. \quad (6)$$

Here the matrices $Z_\infty, F_{12\infty}, F_{2\infty}$ and $L_{2\infty}$ are described in [17] p.p. 451-52. We define the estimate $\hat{d}$ of the deflection signal $\tilde{d}$ by $\hat{d} \triangleq \hat{e} - e$, where $\hat{e} = C_2\hat{x} + D_{22}u$ is the estimate of the error, e. Therefore, if we define the state estimation error, $\tilde{x} \triangleq x - \hat{x}$ and the profile estimation error by $e_d \triangleq \hat{d} - \tilde{d}$, then

$$e_d = \hat{d} - \tilde{d} = (C_2\hat{x} + D_{22}u) - (C_2 x + D_{22}u - \tilde{d}) - \tilde{d} = -C_2\tilde{x}$$

From Equations (4) and (5), we have

$$\begin{aligned}
\dot{\tilde{x}} &= A\tilde{x} + B_1(w - F_{12\infty}\hat{x}) + Z_\infty L_{2\infty} F_{12\infty}\tilde{x} + Z_\infty L_{2\infty}(d - F_{12\infty}\hat{x}) \\
\Rightarrow E_d(s) &= -C_2\tilde{x}(s) \\
&= -(\underbrace{C_2(sI - A - Z_\infty L_{2\infty} C_2)^{-1} B_1(w - F_{12\infty}\hat{x})}_{\triangleq E_1(s)} + \\
&\quad \underbrace{C_2(sI - A - Z_\infty L_{2\infty} C_2)^{-1} Z_\infty L_{2\infty}(d - F_{12\infty}\hat{x})}_{\triangleq E_2(s)}).
\end{aligned}$$

Since, $e_d = -C_2\tilde{x}$, and $\tilde{x}$ is the state of a stable system, we expect the e_d to be small. But we prove a stronger result (see Appendix): that $E_1(s) = 0$ and $E_2(s) = 0$ by exploiting the structure of the generalized plant!

This means that $E_d(s) = 0$ which implies that $\hat{d}$ tracks $\tilde{d}$ of arbitrarily large frequencies. In typical AFM designs the estimates of the sample profile, $\tilde{d}$ is obtained by processing the control signal u (as in 'constant force mode') or the deflection signal y_m (as in the 'constant height mode'). The profile estimate $\hat{d}$, on the other hand, derives information from *both* u and y_m. Note that $\hat{d}$ is prescribed only in terms of signals arising out of design of K_1. Also since $E_d(s) = -(K_2S + 1)\tilde{d} = 0$, therefore $K_2S = -1$. In this context the profile estimate using $\mathcal{H}_\infty$ design does provide many advantages: (a) it is easy to design as there is plenty of commercial software that solves these optimal control problems and (b) as the signal estimate transfer function K_2 in Figure 3 comes as a consequence of design of K_1 and does not require any explicit computation- i.e. the profile estimate $\hat{d}$ is prescribed in terms of the internal signals ($\hat{e}$ and e) in the loop itself and thus does not add to the computational burden in the design procedure. Another important aspect of this design is that the class of controllers that attain the first three objectives are given by lower Linear Fractional Transformation (LFT) $\mathcal{F}_l(K_1, Q)$ where $Q(s)$ is any stable proper transfer function such that $\|Q\|_\infty \leq \gamma$ where γ is performance bound as described at the end of the section 1. Since K_2 is completely specified by K_1, this also gives a parametrization of all the controllers that satisfy all the objectives in (2).

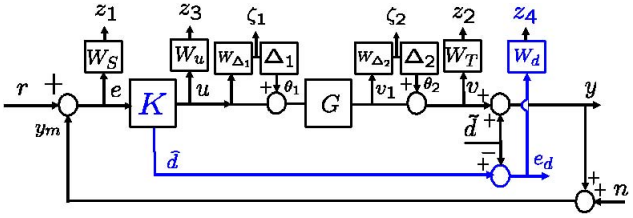

Figure 4. THE SCHEMATIC FOR THE ROBUST $\mathcal{H}_\infty$ FRAMEWORK WITH OUTPUT AND INPUT MULTIPLICATIVE PLANT UNCERTAINTIES.

1.2 Robustness of this signal to plant uncertainties

An important aspect of control design in AFM is robustness. It is especially important since the unmodeled nonlinear effects of piezoactuation such as drift and hysteresis are significant; and these devices are used in diverse operating conditions which necessitate robustness to these uncertainties. We consider a modified block diagram shown in Figure 4 to study robustness of the prescribed control design with respect to modelling uncertainties. In this model G is modified to include input and output multiplicative uncertainties. The matrix transfer function from $[r - n\ \tilde{d}]$ to the vector of regulated variables $z \triangleq [z_1\ z_2\ z_3\ z_4]^T$ (is the same as given in (1)) describes the nominal performance. The control design prescribed in previous section ensures that the transfer functions $\|W_S S\| < 1$, $\|W_T T\| < 1$ and $\|W_u K_1 S\| < 1$. Moreover, the proposed choice of K_2 is such that $K_2 S = -1$. Thus by choosing the weighting function W_d such that it is small at those frequencies where noise is significant we guarantee all the nominal performance objectives. The noise n and the disturbance $\tilde{d}$ are indistinguishable to the controller and therefore an appropriate filter W_d is required to separate out the two. The transfer function from perturbation inputs $\theta \triangleq [\theta_1\ \theta_2]$ to the regulated variables z describes the robust performance:

$$\begin{bmatrix} z_1 \\ z_2 \\ z_3 \\ z_4 \end{bmatrix} = \begin{bmatrix} -W_S GS & -W_S S \\ W_T GS & -W_T S \\ -W_u T & W_u K_1 S \\ -W_d G K_2 S & -W_d K_2 S \end{bmatrix} \begin{bmatrix} \theta_1 \\ \theta_2 \end{bmatrix}.$$

The control design for nominal performances for set point regulation, boundedness of control, and profile estimation error also guarantees robustness with respect to output uncertainty (with θ_2). The effect of θ_2 on z_2 given by $W_T S$ is not small but this is expected as this model fails to distinguish the output uncertainty (θ_2 which is akin to sensor noise) and the disturbance signal $\tilde{d}$.

The robustness to input uncertainty (to θ_1) suggests a careful design of K to account for the trade off between nominal and robust performances. Thus designing W_S, W_T and W_d so that they shape GS, GK_1S and GK_2S instead of S, K_1S and K_2S respectively ensures robust performance of bandwidth, boundedness of control and profile estimation with respect to the input uncertainty. This is evident from the fact that in SISO system we can easily lump together the input and ouput uncertainties by transferring the input uncertainties to the output side via the plant transfer function G [16]. The transfer function from θ_2 to $[z_1\ z_2]^T$ further shows that there is a trade off between the robustness in set point regulation and high resolution with respect to input uncertainty. This trade off is captured by the fact that robust performance of both requires W_SGS and W_TGS to be small simultaneously. The transfer function from $[\theta_1\ \theta_2]^T$ to e_d evaluates robust performance of the proposed design. Note that since $1+K_2S=0$, W_d needs to be chosen so as to make W_d small at the frequencies where n and θ_2 are significant and to make W_dG small at those frequencies where θ_1 is significant. This can easily be incorporated without making any compromise on the transfer function from sample profile $\tilde{d}$ to the estimation error z_4 which remains equal to zero!

It should be emphasized that input uncertainty is not as significant as the output uncertainty as illustrated in Section 3.

2 Observer Based Designs

The $\mathcal{H}_\infty$ design presented here finds a solution to an optimal problem which makes it unnecessary to study other designs. However, the model in which the sample profile is viewed as a disturbance signal as in Figure 2 immediately suggests an observer based design for disturbance estimation. Also the similarity in the structures of the controllers in $\mathcal{H}_\infty$ and the observer designs gives a good motivation to study the latter. The various trade offs between the regulation, robustness and profile estimation have close analogues in the $\mathcal{H}_\infty$ design. This provides a good motivation to study observer based designs. In this section we propose profile estimate signals based on observer based designs and analyze them.

A schematic of this design is illustrated in Figure 5(A). The basic idea is to exploit the difference between the deflection signal $e=C_2x+\tilde{d}$ (where $\bar{d}=\tilde{d}+n$, the notation for states and generalized plant is the same as in (4)) and its estimate $\hat{e}=C_2\hat{x}$. Therefore, when the state estimate error $x-\hat{x}$ goes to zero - the corresponding difference in deflection signal $\hat{d}\stackrel{\triangle}{=}\hat{e}-e$ goes to $\bar{d}$; or equivalently the profile estimation error $e_d\stackrel{\triangle}{=}\hat{d}-\tilde{d}$ goes to zero. The control design is translated to finding gain matrices F and L such that the profile estimation error e_d is small while maintaining the deflection signal at the set point and at the same time ensuring robustness of these objectives to modeling uncertainties in G. In this context we analyze the following cases:

Model with Multiplicative Uncertainty Here a multiplicative uncertainty is considered (see Figure 5(B)) similar to the model in Figure 4. In this model, the disturbance $\tilde{d}$, the noise n and the uncertainty θ_2 are indistinguishable. If we represent $\bar{d}\stackrel{\triangle}{=}n+\tilde{d}$, then the transfer function from $[\bar{d}-\theta_2\ \theta_1]^T$ to $[e_d\ z_1\ \zeta_1\ \zeta_2]^T$ is equal to

$$\begin{bmatrix} 1 & & \\ -\frac{W_S}{1+\Gamma_1\Gamma_2} & & \\ & -\frac{W_{\Delta_1}}{1+\Gamma_1\Gamma_2} & \\ & & -\frac{W_{\Delta_2}\Gamma_1}{1+\Gamma_1\Gamma_2} \end{bmatrix} \begin{bmatrix} -C_g\Omega_L^{-1}L_1 & -C_g\Omega_L^{-1}B_g \\ 1-F\Gamma_4^{-1}(B_1-L) & \Gamma_1(1-F\Gamma_4^{-1}B_2) \\ \Gamma_2+\Gamma_3+(\Gamma_3+1)F\Gamma_4^{-1}(B_1-L) & (\Gamma_3-\Gamma_1\Gamma_2)-(\Gamma_3+1)F\Gamma_4^{-1}B_2 \\ \Gamma_2-F\Gamma_4^{-1}(B_1-L) & 1-F\Gamma_4^{-1}B_2 \end{bmatrix},$$

where $F=[F_1\ \ F_2], L=[L_1\ \ L_2]^T, \Omega_L=sI-A_g-L_1C_g, \Omega_F=sI-A_g-B_gF_1, \Gamma_1=C_g\Omega_F^{-1}B_g, \Gamma_2=F_2(sI-A_s)^{-1}B_s, \Gamma_3=F_1\Omega_F^{-1}B_g$ and $\Gamma_4=sI-A-LC_2$ and the other matrices are defined in (3) and (4).

Note that the sensitivity of the profile estimation error on $[\bar{d}+\theta_2\ \theta_1]^T$ depends solely on L_1. By making use of the structure of B_1 and setting $L=B_1$ which implies $L_1=0$, the transfer function from $\bar{d}+\theta_2$ to e_d is zero, i.e. $T_{e_d\bar{d}}=0$. Therefore we have zero profile estimation error. However the robustness of this signal with θ_1 is solely dictated by the plant G. Thus the design of L captures the trade off between nominal and robust performance of the profile estimate signal. The design of F for this choice of L is more complicated. A first try at it can be done by setting $F_2=0$ which gives $\Gamma_2=0$ which in turn implies $T_{\zeta_2\bar{d}}=0$ and therefore guarantees robustness - i.e. the sensitivity of ζ_2 to $\bar{d}$ and θ_2 is zero. These results are deceptive since the profile estimate does not distinguish the profile $\tilde{d}$ from the noise n or the uncertainty θ_2. Furthermore this choice of parameters gives $T_{z_1\bar{d}}=-W_S$ which implies that the set point regulation becomes independent of the gain F. Thus $F_2=0$ is not an appropriate choice and the design of F_2 captures the trade off between set point regulation and robustness to the output uncertainty. This analysis gives insights into relative roles of F and L with respect to profile estimation, regulation and robustness but it does not give an easy methodology to compute the gain F. The design of F and L to simultaneously address all these objectives proves to be significantly complex. As a result, here we do not analyze the set point regulation and the robustness of ζ to θ but concentrate only on the performance of the sample profile estimation. $T_{e_d\bar{d}}=C_g(sI-A_g-L_1C_g)^{-1}L_1$ and $T_{e_d\theta_1}=C_g(sI-A_g-L_1C_g)^{-1}B_g$ capture the nominal and the robust performance objectives with respect to profile estimation. Ideally we would like to have both these transfer functions small. We interpret the trade off between nominal and robust performance in terms of an auxiliary system and design L_1 by solving a Linear Quadratic Regulator (LQR) problem based on the auxiliary system which is described by

$$\begin{aligned} \dot{\xi} &= A_g^T\xi+C_g^Tw+C_g^Tu \\ y &= \xi \\ z_a &= u \\ z_b &= B_g^T\xi. \end{aligned}$$

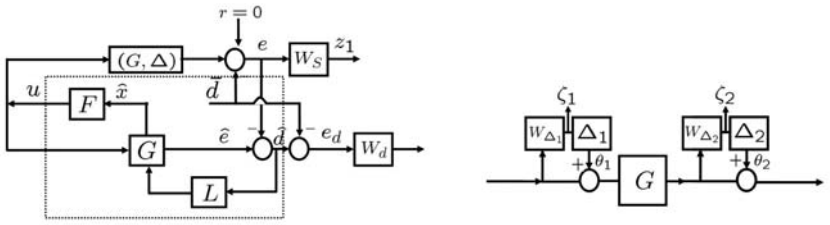

(A) (B)

Figure 5. (A) A SCHEMATIC OF THE OBSERVER DESIGN (B) THE FORM OF (G,δ) FOR INPUT AND OUTPUT MULTIPLICATIVE UNCERTAINTIES.

The control law that results from the Linear Quadratic Regulator problem with the cost function:
$\int_0^\infty \xi^T B_g Q B_g^T \xi + u^T R u dt$ is given by $u = R^{-1} C_g Z \xi$ where Z satisfies the Algebraic Riccati Equation (ARE)

$$A_g Z + Z A_g^T - Z C_g^T R^{-1} C_g Z + B_g Q_g B_g^T = 0.$$

If we define $L_1^T = R^{-1} C_g Z$, then $z_a = L_1^T \xi$ and consequently $T_{z_a w} = C_g (sI - A_g - L_1 C_g)^{-1} L_1 = T_{e_d, \hat{d}}$ and $T_{z_b w} = C_g (sI - A_g - L_1 C_g)^{-1} B_g = T_{e_d \theta_1}$. Thus the LQR trade off between having small z_a and z_b signals of the auxiliary system translates to the trade off between nominal and robust sample estimation performance of the original system. The relative importance of the nominal and robust performances is determined by appropriate choice of Q and R. The relative importance between the input and output uncertainties can be used to decide relative magnitudes of Q and R.

This design helps only in the design of L. The design of F to appropriately decide the trade off between regulation and robustness is not easy. It would require setting up of an optimization problem and its solving which the $\mathcal{H}_\infty$ design incorporates and solves right from the beginning.

3 Experimental Setup and Results

The experiments were performed using MFP-3D developed by *Asylum Research Inc., Santa Barbara, CA*. The transfer function from u, the input to the Z-piezo, to the measured output y_m was obtained using frequency domain based identification techniques. . The frequency response of the device at this operating point over a 2 kHz bandwidth is shown in the bode plot (dashed lines) in Figure 6. Accordingly, an eleventh order stable transfer function was fit to this data. Figure 6 shows that there is a good match between this frequency response data and the one fitted to the data, $G(s)$.

The control transfer function K_1 was obtained using the *hinf* function in MATLAB. In this design, the weighting function W_S was chosen to be a first order transfer function, $W_s(s) = \frac{0.3333s+2199}{s+2.199}$. This transfer function is designed so that its inverse (an approximate upper bound on the sensitivity function) has a gain of $-60dB$ at low frequencies (< 100 *Hz*) and a gain of $\approx 9.5dB$ above 1000 Hz. The weight W_T was chosen to be $W_T(s) = \frac{s+2199}{10^{-5}s+1.1\times10^4}$ which has high gains (100 dB) at high frequencies (note that noise is in the high frequency region) to ensure high resolution. The transfer function, $K_1 S$ was scaled by a constant weighting W_u =40 dB, to restrict the magnitude of the input signals such that they are within the saturation limits. This weighting constant gives control signals that are at most six times the reference signals.

The $\mathcal{H}_\infty$ design resulted in controllers given by K_1 and K_2. Figure 7(B) shows the controller and observer obtained from the solution of stacked H_∞ problem. Note that K_1 and K_2 have a similar dynamics at low frequencies and therefore give similar images at these frequencies. These transfer functions were implemented on the DSP and the signals $\hat{d}, r$, and u were recorded and used to evaluate images. Figure 8 shows experimental and theoretical frequency response of sensitivity and complementary sensitivity functions. As seen in the figures, experimental and theoretical responses match closely except a particular frequency range around 400 Hz.

To study the performance of the new estimate signal, it was compared to and contrasted with the typically used control signal. Figure 9(A) shows that the bandwidth of the transfer function T_{ud} has a bandwidth of approximately 800 Hz where as the magnitude of $T_{\hat{d}d}$ (in Figure 9(B)) is within 3 dB for the whole range considered. The phase plots show considerable phase drop for the T_{ud} while near zero phase for the $T_{\hat{d}d}$. This explains the difference seen in the trace and the retrace scans when using the u signal for the image. It is important to note that the bandwidth of 800 Hz for the transfer function T_{ud} is by itself a huge improvement over typical commercial AFMs (which have imaging bandwidth in order of few tens of Hertz).

In addition to investigating the above transfer functions, imaging experiments were performed to test the proposed profile estimate signal. A gold calibration grid with squares of height 180 nm every 10 μm was used for imaging using the $\hat{d}$ signal. This image was compared with the one obtained from the con-

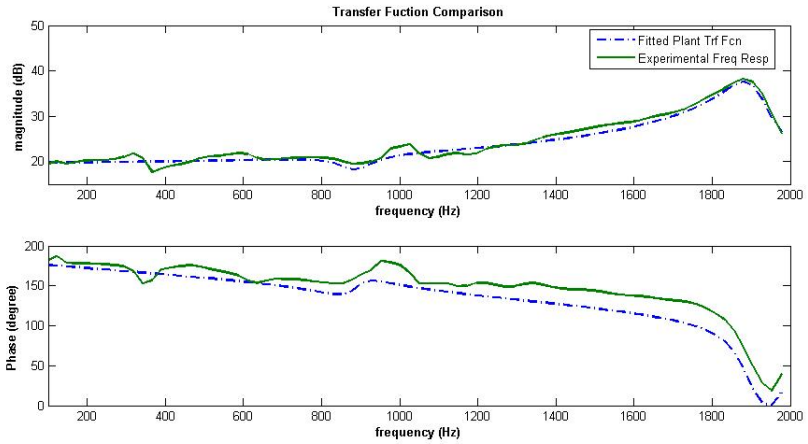

Figure 6. EXPERIMENTALLY (SOLID) OBTAINED FREQUENCY RESPONSE IS COMPARED WITH THAT OF THE MODEL (DOTTED) G.

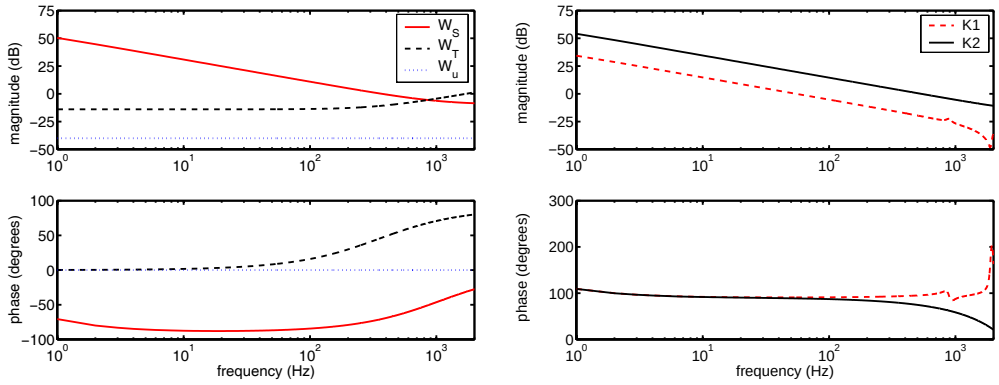

Figure 7. CONTROL DESIGN: (A) WEIGHTING FUNCTIONS FOR SENSITIVITY, COMPLEMENTARY SENSITIVITY AND ACTUATION SIGNAL (W_S, W_T AND W_u) RESPECTIVELY (B) TRANSFER FUNCTIONS OF CONTROLLER K_1 AND OBSERVER K_2 OBTAINED FROM $HINFSYN$ DESIGN.

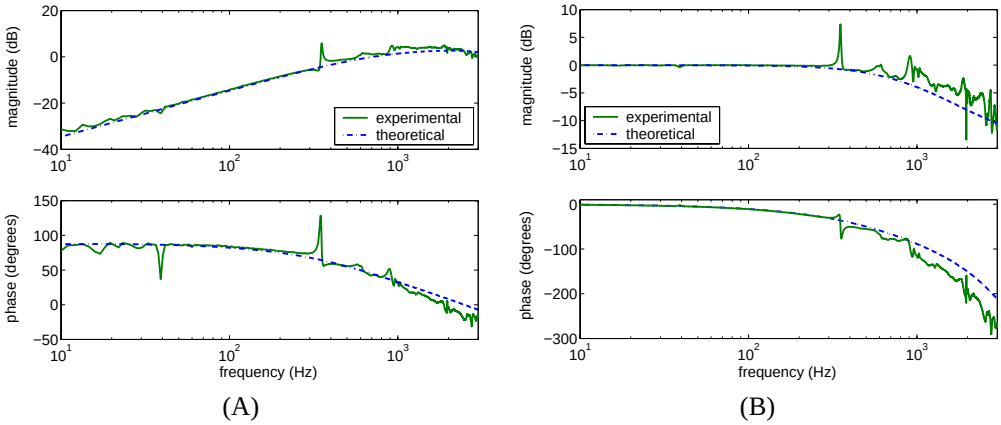

Figure 8. EXPERIMENTAL VALIDATION: (A) AND (B) THE PLOT COMPARES THE SIMULATED AND THE EXPERIMENTALLY OBTAINED SENSITIVITY AND COMPLEMENTARY SENSITIVITY TRANSFER FUNCTIONS RESPECTIVELY. THERE IS A GOOD MATCH BETWEEN THE TWO.

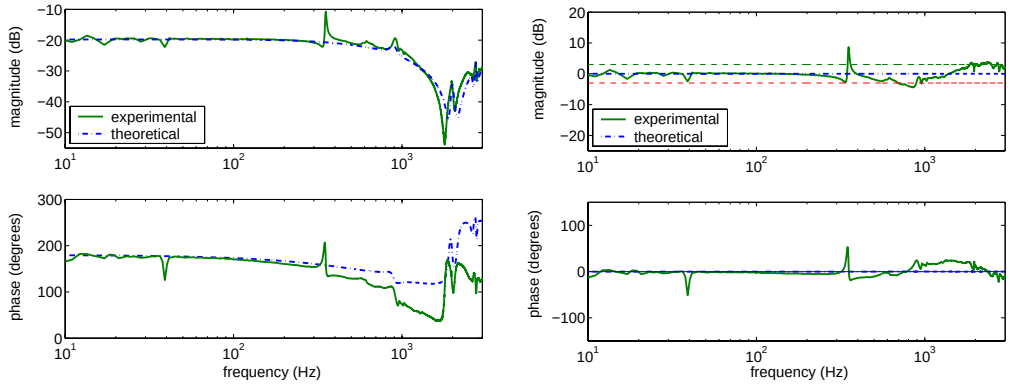

(A) (B)

Figure 9. (A) THE EXPERIMENTAL FREQUENCY RESPONSE OF THE CONTROL EFFORT u TO SAMPLE TOPOGRAPHY SHOWING THAT IT IS NOT A GOOD ESTIMATE OF TOPOGRAPHY AT HIGH FREQUENCIES. (B) THE EXPERIMENTAL FREQUENCY RESPONSE OF THE ESTIMATE $\hat{d}$ TO SAMPLE TOPOGRAPHY REMAINS FLAT CORROBORATING THE ANALYTICAL RESULT THAT THIS TRANSFER FUNCTION IS A CONSTANT, THE MAGNITUDE PLOT IS WITHIN ± 3 dB AND THE PHASE IS NEAR ZERO OVER THE ENTIRE RANGE.

trol signal u. In the first experiment, the grating was scanned at 10 Hz and the corresponding control signal u and the proposed estimate signal $\hat{d}$ were recorded. The control signal was proportional to the profile, in fact $u \approx -0.1d$. Therefore u signal was magnified by ≈ 10 times to get the profile estimate. The resulting data is shown in Figure 10(A). Note that the scanned image with the proposed signal is superior to the image with the u signal. This is more evident in the plots showing a particular line scan, where the image with u has an oscillatory behavior in response to the higher frequency content of the square profile. The main feature of the proposed signal is the high bandwidth it achieves. The difference in performance between the $\hat{d}$ and u signals is much greater in faster scans. This is shown in Figure 10(B). Here the scan was done at 150 Hz, 500 Hz and 1400 Hz where the reference signal was generated on the computer itself and downloaded onto the DSP card to mimic a sinusoidal sample profile.

At low frequencies (below the bandwidth of T_{ud}) the control signal u is a good measure of d. However, there is a significant phase lag between the d and the u signal at 500 Hz. At higher frequency (1400 Hz) control signal gives a poor estimate of d - it is attenuated (by more than 50%) and has considerable phase lag. The experimental results show that the proposed signal $\hat{d}$ tracks near perfectly the reference signal even at these high bandwidths, as well as in lower frequencies. This fact is corroborated from the frequency response of transfer functions shown in Figure 9, where T_{ud} rolls off after 800 Hz with significant phase lag but $T_{\hat{d}d}$ remains with ± 3 dB with almost zero phase. This imaging at 1.4 kHz demonstrates a substantial improvement over the existing technology where images are usually scanned at few tens of Hertz.

This same algorithm was also implemented on another AFM (Veeco Instruments, Santa Barbara, CA) and experimental results again corroborated that $T_{\hat{d}d} \approx 1$ (results not shown here).

4 Conclusions

The imaging problem in an Atomic Force Microscope is addressed using modern control theory. An optimal control problem is formulated to address the design of a new profile estimate signal which is valid even for fast scanning in Atomic Force Microscopy. The objectives of set point regulation and high resolution are also included in the formulation. The solution of this problem yields a new estimate of the sample profile, $\hat{d}$ and it is *proved* that the transfer function from the profile to the estimate is 1. The designed controllers were implemented and a substantial improvement over the traditional designs is shown. Typical controllers in commercial AFMs use PID controllers which do not give reliable images beyond a few tens of Hertz bandwidth while experiments with the proposed signal at 1400 Hz gave faithful images. Experiments show a significant improvement in bandwidth in sample-profile estimation. The proposed signal makes use of *both* the control signal u and the deflection signal e smartly to give the sample profile in contrast to using only the control signal u in constant force imaging and using only the deflection signal e in constant height imaging.

Advanced control tools have been used to tackle an important problem in atomic force microscopy. This work further demonstrates the immense scope for control theoretic tools to improve the bandwidth, resolution and reliability of these devices.

Proof for $E_1(s) = 0$ and $E_2(s) = 0$ This derivation relies on the structure of the generalized plant P and the quasi-observer

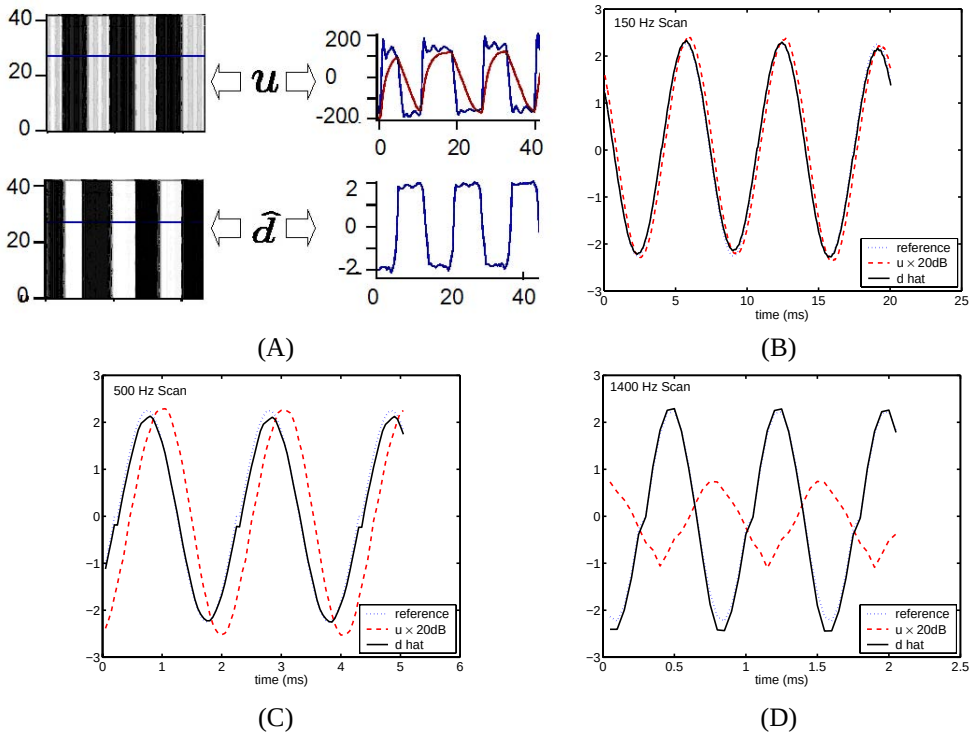

Figure 10. (A) EXPERIMENTAL DATA SHOWING SIGNIFICANTLY SUPERIOR IMAGES (LEFT PANEL) OBTAINED BY USING THE NEW IMAGING SIGNAL $\hat{d}$ COMPARED TO THE USE OF THE CONTROL EFFORT u AS THE SAMPLE TOPOGRAPHY ESTIMATE. (B,C): THE u SIGNAL GIVES WORSE ESTIMATES AS THE FREQUENCY IS INCREASED (150 HZ AND 500 HZ). THE $\hat{d}$ SIGNAL HAS PRACTICALLY NO PHASE LAG. (D) EXPERIMENTAL DATA THAT SHOWS THAT THE NEW IMAGING SIGNAL $\hat{d}$ FOLLOWS A 1.4 KHZ REFERENCE SINE WAVE THAT THE CONTROL SIGNAL IS UNABLE TO TRACK AT ALL.

form of the $\mathcal{H}_\infty$ controller developed in [17] p.p. 451-452. The transfer function, G is proper which implies that $D_{22} = D_g = 0$. This coupled with structure of P, when substituted in equations give $Z_\infty = I$ and $L_{2\infty}$ is product of B_1 and another matrix, i.e. $Z_\infty L_{2\infty}$ is of the form $B_1\times$. This implies that both E_1 and E_2 are of the form $C_2(sI-A-Z_\infty L_{2\infty}C_2)^{-1}B_1\times$ and therefore it is enough to show that $C_2(sI-A-Z_\infty L_{2\infty}C_2)^{-1}B_1 = 0$.

By using that A is stable and the identity $(I-uv')^{-1} = (I + uv'/(1-v'u))$ for column vectors u and v, we show that

$$C_2\ (sI-A-Z_\infty L_{2\infty}C_2)^{-1}B_1 \tag{7}$$

$$= C_2(sI-A)^{-1}\left(I - \underbrace{Z_\infty L_{2\infty}}_{u}\underbrace{C_2(sI-A)^{-1}}_{v'}\right)^{-1} B_1 \tag{8}$$

$$= C_2(sI-A)^{-1}\left(I + \frac{Z_\infty L_{2\infty}C_2(sI-A)^{-1}}{1-C_2(sI-A)^{-1}Z_\infty L_{2\infty}}\right)B_1$$

$$= \frac{C_2(sI-A)^{-1}B_1}{1-C_2(sI-A)^{-1}Z_\infty L_{2\infty}}$$

This in turn implies that it is enough to show that $C_2(sI-A)^{-1}B_1 = 0$. Now $C_2 = \begin{bmatrix} -C_g & 0 \end{bmatrix}$ and A is of lower block triangular form $A = \begin{bmatrix} A_g & 0 \\ \times & \times \end{bmatrix}$ and B_1 is of the form $\begin{bmatrix} 0 \\ \times \end{bmatrix}$. After noting that $(sI-A)^{-1}$ is itself a lower block triangular matrix,

$$C_2(sI-A)^{-1}B_1 = \begin{bmatrix} -C_g & 0 \end{bmatrix}\begin{bmatrix} (sI-A_g)^{-1} & 0 \\ \times & \times \end{bmatrix}\begin{bmatrix} 0 \\ \times \end{bmatrix} = 0$$

Hence $E_1(s) = 0$ and $E_2(s) = 0$.

REFERENCES

[1] Sebastian, A., Salapaka, M., Chen, D., and Cleveland, J., 2001. "Harmonic and Power balance tools for tapping-mode AFM". *Journal of Applied Physics*, **89**(11), June, pp. 6473–80.

[2] Lee, S.-I., Howell, S., Raman, A., and Reifenberger, R., 2002. "Nonlinear dynamics of microcantilevers in tapping mode atomic force microscopy- comparison between theory and experiment". *Physical Review B*, **66**(11).

[3] Ashhab, M., Salapaka, M., Dahleh, M., and Mezic, I., 1999. "Dynamical analysis and control of micro-cantilevers". *Automatica*, **35**(10), October, pp. 1663–70.

[4] Salapaka, S., Dahleh, M., and Mezic, I., 2001. "On the dynamics of a harmonic oscillator undergoing impacts with a vibrating platform". *Nonlinear Dynamics*, **24**, December, pp. 333–358.

[5] Salapaka, M., Bergh, H., Lai, J., Majumdar, A., and McFarland, E., 1997. "Multimode noise analysis of cantilevers for scanning probe microscopy". *Journal of Applied Physics*, **81**(6), pp. 2480–87.

[6] Schitter, G., Menold, P., Knapp, H. F., Allgower, F., and Stemmer, A., 2001. "High performance feedback for fast scanning atomic force microscopes". *Review of Scientific Instruments*, **72**(8), August, pp. 3320–3327.

[7] Sebastian, A., Cleveland, J., and Salapaka, M., 2003. "Robust Control Approach to Atomic Force Microscopy". *to appear in Conference on Control and Decision, Hawaii*, December.

[8] Salapaka, S., Sebastian, A., Cleveland, J. P., and Salapaka, M. V., 2002. "High bandwidth nano-positioner: A robust control approach". *Review of Scientific Instruments*, **73**(9), September, pp. 3232–3241.

[9] Daniele, A., Salapaka, S., Salapaka, M., and Dahleh, M., 1999. "Piezoelectric scanners for atomic force microscopes: Design of lateral sensors, identification and control". In Proceedings of the American Control Conference, San Diego, California, pp. 253–257.

[10] Croft, D., Shedd, G., and Devasia, S., 2000. "Creep, Hysteresis and Vibration compensation for Piezoactuators: Atomic Force Microscopy Application". In Proceedings of the American Control Conference, Chicago, Illinois, pp. 2123–2128.

[11] Sahoo, D., Sebastian, A., and Salapaka, M., 20013. "Transient Signal based sample-detection in Atomic Force Microscopy". *American Physics Letters*, **83**(26), p. 55215523.

[12] Napoli, M., Bamieh, B., and Dahleh, M., 1999. "Optimal control of arrays of microcantilevers". *Journal of Dynamic Systems Measurement and Control*, **121**, December, pp. 686–690.

[13] Napoli, M., Bamieh, B., and Turner, K., 2003. "Mathematical modeling, experimental validation and observer design for a capacitively actuated microcantilever". *Proceedings of the American Control Conference, Denver, CO*, June 4-6.

[14] Croft, D., Shedd, G., and Devasia, S., 2001. "Creep, hysteresis and vibration compensation for piezoactuators: Atomic force microscopy application". *Journal of Dynamic Systems, Measurement and Control*, **123**, pp. 35–43.

[15] Sebastian, A., and Salapaka, S., 2003. "$\mathcal{H}_\infty$ loop shaping design for nano-positioning". In Proceedings of the American Control Conference, Denver, CO, pp. 3708–3713.

[16] Skogestad, S., and Postlethwaite, I., 1997. *Multivariable Feedback Control, Analysis and Design*. John Wiley and Sons.

[17] Zhou, K., Doyle, J., and Glover, K., 1996. *Robust and Optimal Control*. Prentice Hall, Upper Saddle River, NJ 07458.

[18] Doyle, J., Glover, K., Khargonekar, P., and Francis, B., 1989. "State-space solutions to standard H_2 and H_∞ control problems". *IEEE Transactions on Automatic Control*, **34**(8), August, pp. 831–847.

[19] Glover, K., and McFarlane, D., 1989. "Robust stabilization of normalized coprime factor plant descriptions with $\mathcal{H}_\infty$-bounded uncertainty". *IEEE transactions on automatic control*, **34**(8), August, pp. 821–830.

[20] McFarlane, D., and Glover, K., 1992. "A loop shaping design procedure using $\mathcal{H}_\infty$ synthesis". *IEEE transactions on automatic control*, **37**(6), June, pp. 759–769.

[21] Sefton, J., and Glover, K., 1990. "Pole/zero cancellations in the general $\mathcal{H}_\infty$ problem with reference to a two block design". *Systems and Control Letters*, **14**(4).